Quasi-two-dimensional antiferromagnet on a triangular lattice $RbFe(MoO_4)_2$

L. E. Svistov, A. I. Smirnov, and L. A. Prozorova
P. L. Kapitza Institute for Physical Problems RAS, 117334 Moscow, Russia

O. A. Petrenko
Department of Physics, University of Warwick, Coventry, CV4 7AL, United Kingdom

L. N. Demianets and A. Ya. Shapiro
A. V. Shubnikov Institute for Crystallography RAS, 117333 Moscow, Russia

(Received 10 October 2002; revised manuscript received 24 January 2003; published 31 March 2003)

$RbFe(MoO_4)_2$ is a rare example of a nearly two-dimensional Heisenberg antiferromagnet on a triangular lattice. Magnetic resonance spectra and magnetization curves reveal that the system has a layered spin structure with six magnetic sublattices. The sublattices within a layer are arranged in a triangular manner with the magnetization vectors 120° apart. The *H-T* phase diagram, containing at least five different magnetic phases is constructed. In zero field, $RbFe(MoO_4)_2$ undergoes a phase transition at $T_N = 3.8$ K into a noncollinear triangular spin structure with all the spins confined in the basal plane. The application of an in-plane magnetic field induces a collinear spin state between the fields $H_{c1} = 47$ kOe and $H_{c2} = 71$ kOe and produces a magnetization plateau at one-third of the saturation moment. Both the ESR and the magnetization measurements also clearly indicate an additional first-order phase transition in a field of 35 kOe. The exact nature of this phase transition is uncertain.

DOI: 10.1103/PhysRevB.67.094434 PACS number(s): 76.50.+g, 75.50.Ee, 75.30.Cr

I. INTRODUCTION

The problem of an antiferromagnet on a triangular planar lattice (AFMT) has been intensively studied theoretically.[1–5] The ground state in the Heisenberg and *XY* models is a ''triangular'' planar spin structure with the three magnetic sublattices arranged 120° apart. The orientation of the spin plane is not fixed in the exchange approximation in the Heisenberg model.

A nonzero magnetization appears in the presence of a magnetic field due to the canting of the sublattices. Possible field-induced structures are shown in Fig. 1. All configurations with equal magnetization vectors but with different sublattice orientations have the same energy in the molecular field approximation when taking the exchange interaction in the Heisenberg form.[5] The umbrellalike structure *a* with the sublattices tilted from the spin plane towards the field, and the planar structures *b* and *b'* are among these degenerate configurations. In this approximation the *b* configuration becomes collinear (*c* configuration) at a particular field $H_c = H_{sat}/3$, where H_{sat} is the saturation field. In magnetic fields above H_c, the structure is again noncollinear, with two parallel sublattices tilted with respect to the third, forming the ''canted'' *d* phase. Finally, at the saturation field $H = H_{sat}$, a spin-flip transition to the phase *f* occurs.

Because of the degeneracy of the classical spin configurations, both quantum and thermal fluctuations play an important role in the formation of the equilibrium state of the AFMT.[2,5,6] They result in a free-energy gain of the planar structure with respect to the umbrellalike structure. Due to the contribution of fluctuations to the free energy the more symmetric configuration *b* is preferred to *b'*. Further, the fluctuations stabilize the collinear spin configuration *c* in a range of magnetic fields $H_{c1} \leqslant H \leqslant H_{c2}$ around the special point $H = \frac{1}{3} H_{sat}$. Thus, a magnetization plateau should be observed over a relatively wide field range.

In the case of an easy-plane magnetic anisotropy, an analogous evolution of the sublattice orientations is expected when a magnetic field is applied in the easy plane. The spin-flop transition with the rotation of the spins perpendicular to the magnetic field, usually observed in antiferromagnets, is not expected here because the susceptibility is nearly isotropic. The umbrellalike structure should be realized for magnetic fields applied along the sixfold axis C^6, provided the easy-plane anisotropy is sufficiently strong.

The magnetic resonance spectrum of a 120°-spin structure differs from the spectrum of a usual antiferromagnet both in the number of normal modes and in the dependencies of frequencies on the applied magnetic field. There are three eigenmodes for a two-dimensional (2D) triangular structure.[5,7] For the case of an easy-plane anisotropy, two of them are degenerate in zero field, but have nonzero frequency; the third mode has zero frequency in zero field. In a magnetic field there are three different resonance frequencies of uniform spin precession.

The presence of the interplanar antiferromagnetic exchange requires one to consider at least a six-sublattice 3D magnetic structures. For a weak interplanar exchange, however, the main features of the 2D system should remain unchanged. The interplane exchange may cause additional field-induced phase transitions, where the mutual orientation of spins in neighboring planes changes. Possible magnetic structures of the 3D *XY* AFMT in a magnetic field were analyzed in Ref. 4, while the Heisenberg AFMT was considered in Ref. 8. A twofold period along the C^6 (or C^3) axis is assumed here. The structures under consideration are shown schematically in Fig. 1 and denoted as $B1$, $B2$, $B3$, C, $D1$, and $D2$. For the zero-field starting structure $B0$ the nearest

 ©2003 The American Physical Society

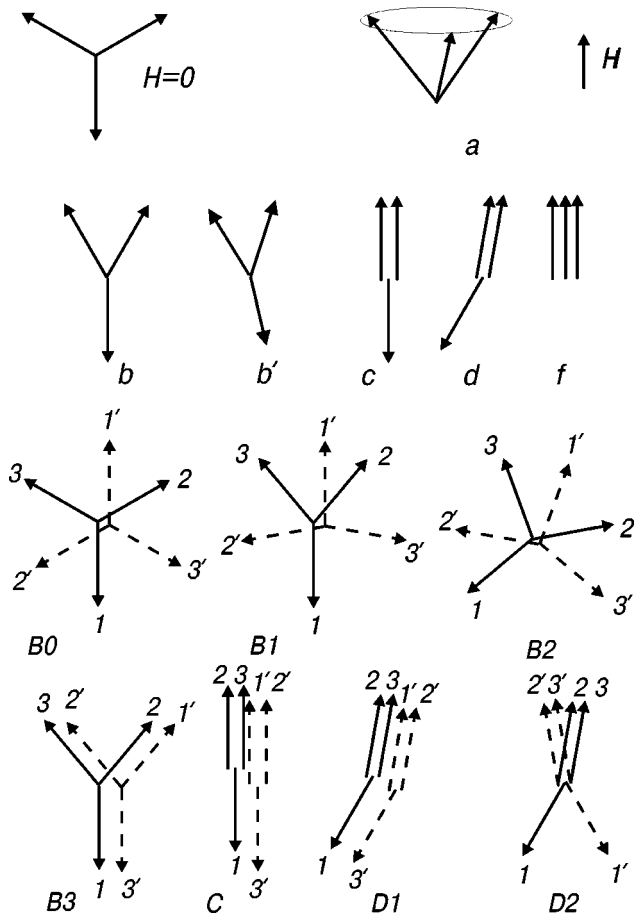

FIG. 1. Schematic representation of the proposed spin structures of a Heisenberg antiferromagnet on a triangular lattice. Structures *a*, *b*, *b′*, *c*, *d*, and *f* are related to the 2D system ($J'=0$). Structures $B0$, $B1$, $B2$, $B3$, C, $D1$, $D2$ represent the triangular antiferromagnet with a weak antiferromagnetic interlayer exchange in the six-sublattice model (Ref. 8): solid and dashed arrows with the same numbers correspond to magnetic moments of neighboring spins from neighboring layers.

neighboring spins, which are placed one above another along the C[6] axis, are considered to be antiparallel due to the antiferromagnetic interplane exchange. Depending on the relative values of the in-plane magnetic field, interplane and intraplane exchange integrals, a phase from the set shown in Fig. 1 should be realized. Thus, for a particular combination of both exchange fields, one might expect a sequence of phase transitions in an increasing magnetic field. Particularly, a sequence of transitions such as $B1$-$B3$-C-$D1$-$D2$-f is possible according to Ref. 8. The last phase corresponds to the parallel orientation of the magnetization of all six sublattices in a high magnetic field. Naturally, the interplanar interaction may also modify the values of the critical fields H_{c1} and H_{c2} with respect to the purely 2D case.[8]

As far as the magnetic resonance spectrum is concerned, the interplanar exchange should result in a splitting of the main eigenfrequencies and in the appearance of new modes due to the increased number of sublattices. There are several materials with triangular lattices carrying magnetic ions, however, the members of the family $A\mathrm{Fe}(TO_4)_2$ ($A=$Cs, Rb; $T=$S, Mo) with $\mathrm{RbFe}(\mathrm{MoO_4})_2$ among them, are the most likely candidates for AFMT systems suitable for experiments. Other related compounds, e.g., the ABX_3 family ($A=$Cs, Rb; $B=$Ni, Mn, Cu; $X=$Cl, Br, I), have an interplanar exchange that is larger than the intraplanar one, thus they are quasi-1D magnets (see, e.g., Refs. 9,10). ''Triangular'' antiferromagnets from other families VX_2 (X=Cl, Br, I) (Ref. 11) and $A\mathrm{CrO_2}$ with $A=$Li, Cu (Ref. 12), have quasi-2D exchange, but their exchange field is too large, shifting the field-induced transitions outside the range of conventional measurements. A review of the magnetic properties of the triangular magnets is given in Ref. 13.

In the present paper, we describe a study of the magnetic and resonant properties of $\mathrm{RbFe}(\mathrm{MoO_4})_2$, a material which can be considered as a rare example of a nearly two-dimensional Heisenberg antiferromagnet on a triangular lattice and that can be prepared in single-crystal form. At room temperature the crystal structure of $\mathrm{RbFe}(\mathrm{MoO_4})_2$ has the space group $P\bar{3}m1$. The magnetic Fe^{3+} ions with spin $S=5/2$ are placed on the hexagonal lattice with lattice parameters $a=5.69$ Å and $c=7.48$ Å. The MoO_4 tetrahedra are placed between the layers of Fe^{3+} ions and form the structure with the threefold axis. The exchange integral J representing the interaction within the planes should be much larger than the exchange integral J' of the nearest neighbor ions in adjacent planes. The large difference in these exchange integrals is due to the different exchange paths of the indirect exchange interactions: via two oxygen ions within the planes and via three or even more oxygen ions between the planes. Thus, the structure of $\mathrm{RbFe}(\mathrm{MoO_4})_2$ may be considered (see, e.g., Ref. 14) as an ensemble of layers with a triangular lattice occupied by $S=5/2$ Fe^{3+} ions, and these magnetic layers are separated by layers of $\mathrm{MoO_4}$-Rb-$\mathrm{MoO_4}$. Magnetic ions in neighboring layers are placed one above another.

Evidence for a structural transformation at $T=180$ K was recently reported in Ref. 15. Small changes of lattice constants, Raman spectra, and ESR linewidth indicate a structural transformation, identified as a second-order phase transition from a highly symmetric $P\bar{3}m1$ room-temperature structure into a very similar but less symmetric $P\bar{3}c1$ low-temperature structure. This transformation corresponds to rotations of the MoO_4 tetrahedra. The ''triangular'' spin structure of Fe^{3+} layers in crystals of $\mathrm{RbFe}(\mathrm{MoO_4})_2$ was recently confirmed by the elastic neutron scattering experiment in zero magnetic field.[16] At the same time, according to the observed neutron diffraction, an incommensurate modulation of the ordered spin structure in the C[3] direction is present there: the mutual orientation of spins from neighboring planes is close to the antiparallel one but is slightly tilted at an angle of 17°. The low-temperature magnetization curves of powder samples of $\mathrm{RbFe}(\mathrm{MoO_4})_2$ were reported earlier.[14] The magnetization saturated at a field of $H_{\mathrm{sat}}=186$ kOe and a magnetization plateau marking the collinear phase was observed. The neutron scattering experiments of Ref. 17 confirming the triangular magnetic structure were performed for powder samples of the related compounds $\mathrm{CsFe}(\mathrm{SO_4})_2$ and $\mathrm{RbFe}(\mathrm{SO_4})_2$.

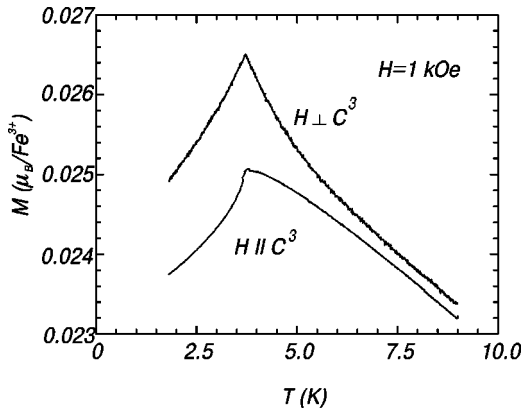

FIG. 2. Temperature dependence of the magnetic susceptibility of $RbFe(MoO_4)_2$ for two directions of the magnetic field.

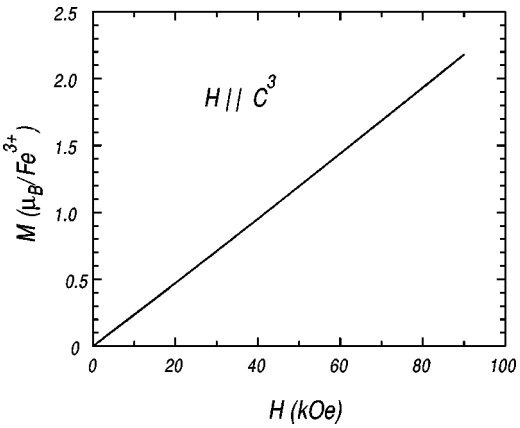

FIG. 3. Field dependence of magnetization of $RbFe(MoO_4)_2$ for $H \| C^3$, $T = 1.6$ K.

We have verified experimentally the theoretical concepts outlined above by taking advantage of single-crystal samples of $RbFe(MoO_4)_2$. The choice of a molybdate instead of a sulphate allowed us to avoid the hydration and to obtain single crystals. Field-induced phase transitions and low frequency spin dynamics in the different phases were studied by means of magnetization measurements and ESR spectroscopy. In the present paper we describe several field-induced phase transitions including transitions not detected earlier. Each phase is found to possess a characteristic set of spin-resonance modes.

II. SAMPLES AND EXPERIMENTAL TECHNIQUES

Single-crystal samples of $RbFe(MoO_4)_2$ were synthesized by means of the spontaneous crystallization from a flux melt. The mixture of $RbFe(MoO_4)_2$ and of $K_2Mo_2O_7$ in the molar ratio of 1:2 was heated in a platinum crucible up to a temperature of 1300 K and held at this temperature for 12 h then cooled to 1000 K at a rate of 3 K/h. The nucleation of crystals was localized due to the temperature gradient near a platinum rod which was inserted into the melt in the precristallization state. The platinum rod was withdrawn from the solution after the crystallization. The $K_2Mo_2O_7$ flux was removed by dissolving in water. A much slower dilution of the crystals of $RbFe(MoO_4)_2$ takes place at the same time. The crystals have the shape of thin hexagonal plates with the size of 3–4 mm along each edge. The lattice parameters are in accordance with those reported for powder samples.[14] The magnetization curves and the temperature dependencies of the magnetic susceptibility were measured using a vibrating sample magnetometer with the field range 0–120 kOe. Magnetic resonance spectra were taken by a set of transmission-type magnetic resonance spectrometers with resonators covering the range 9–120 GHz.

III. EXPERIMENTAL RESULTS

A. Susceptibility and magnetization curves

The temperature dependence of the susceptibility of $RbFe(MoO_4)_2$ at low temperatures is shown in Fig. 2 and clearly demonstrates the transition into the magnetically ordered state at $T_N = 3.8$ K. The susceptibility measurements in the whole range 10–300 K reveal the temperature dependence of the Curie-Weiss type $(T+\Theta_c)^{-1}$ with the value of the Weiss constant $\Theta_c = 22 \pm 2$ K. A small (about 0.1%) steplike anomaly in the inverse susceptibility appears at 180 K giving an additional indication for the structural transformation mentioned in the Introduction. There is a significant deviation from the Curie-Weiss behavior below 10 K. A strong anisotropy of the susceptibility also appears in this temperature range, well above T_N.

Below the transition point $T_N = 3.8$ K, the magnetization curves $M(H)$ are quite different for different orientations of the magnetic field. For $H \| C^3$, the magnetization increases linearly with the field for all values of the applied field (see Fig. 3). For $H \perp C^3$, the field dependence of the magnetization is much more complicated, as shown in Fig. 4 for $T = 1.6$ K. There are abrupt changes in the slope of the magnetization curve at 47 kOe and 71 kOe, with the differential magnetic susceptibility being significantly reduced in the region between these fields.

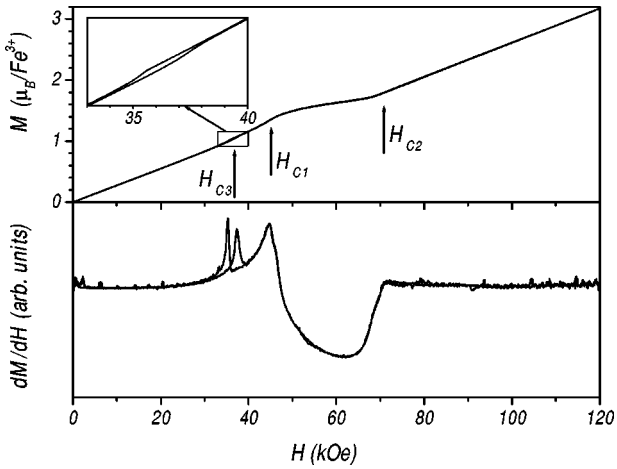

FIG. 4. Field dependence of the magnetization (top panel) and its derivative (bottom panel) of $RbFe(MoO_4)_2$ for $H \perp C^3$, $T = 1.6$ K. The inset shows the hysteresis region around the transition field H_{c3}.

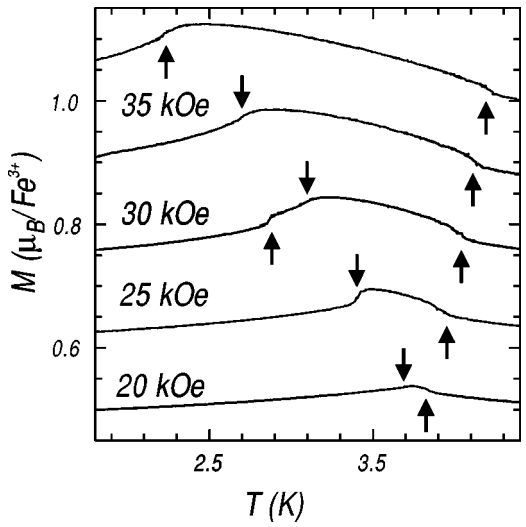

FIG. 5. Temperature dependencies of the magnetization of $RbFe(MoO_4)_2$ in fixed magnetic fields. The arrows mark the temperatures of the abrupt changes of the magnetization corresponding to the magnetic phase boundaries.

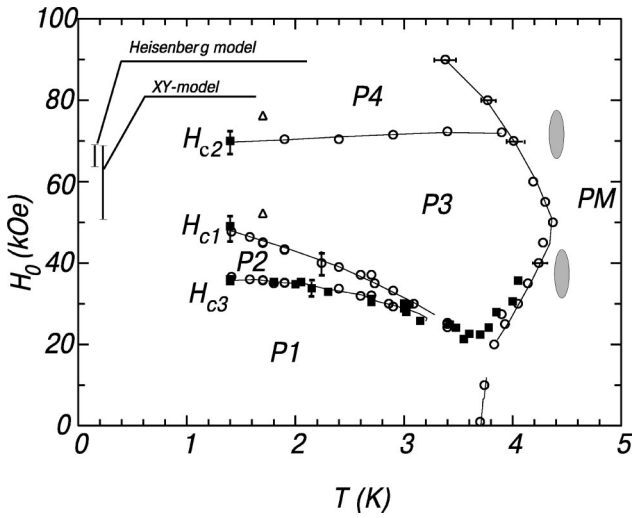

FIG. 6. The H-T magnetic phase diagram of $RbFe(MoO_4)_2$ derived from the single crystal magnetization and ESR measurements. Data marked by triangles are taken from powder measurements (Ref. 14), open circles correspond to magnetization measurements, filled squares - to ESR-data. The two vertical line segments near $T=0$ illustrate the field ranges of the phase "c" according to calculations from Ref. 5 for the Heisenberg and the XY-model. The two shadowed ovals mark the regions of smeared changes in the magnetization slope for $T>T_N$.

An additional, first-order phase transformation with a hysteresis in $M(H)$ curve was detected at $H_{c3}=35$ kOe. Magnetization measured between 30 and 38 kOe shows a large difference in signal obtained for the rising and falling magnetic field. A smaller, but still clearly observable difference exists down to a field of 20 kOe. In order to detect the transitions by changing temperature we measured the temperature dependence of the magnetic moment at constant magnetic field. Several examples of these data are shown in Fig. 5. The temperatures of the abrupt changes of the magnetization curves are marked by arrows and indicate the field dependence of the Néel temperature and the temperature dependence of the fields H_{c1} and H_{c3}. The values of critical magnetic fields and temperatures derived from curves similar to those shown in Figs. 4 and 5 are collected on the H-T phase diagram in Fig. 6. There are at least four ordered antiferromagnetic phases $P1$, $P2$, $P3$, $P4$ and a paramagnetic phase PM.

It should be noted that smeared changes in the magnetization slope were observed at the critical fields H_{c1} and H_{c2} for temperatures slightly above the Néel temperature. These regions are marked in Fig. 6 by shadowed ovals.

B. Antiferromagnetic resonance

On cooling the samples, the ESR line broadens markedly below 10 K. After passing through the Néel point, the ESR line shifts from the paramagnetic resonance position and again becomes rather narrow. The temperature evolution of the ESR line is shown in Fig. 7. In this paper we discuss only the low-temperature magnetic resonance, well below the Néel point. The critical behavior will be the subject of further investigations.

The field dependencies of the microwave transmission at $T=$ 1.3 K are shown in Figs. 8 and 9 for two orientations of the magnetic field. We can derive the field dependencies of the spin-resonance modes in the ordered state from the positions of the resonance-absorption lines at different frequencies. As shown in Fig. 9, the microwave absorption data are sensitive to all the phase transitions detected in the magnetization measurements. The hysteresis loop around the field H_{c3} is clearly evident in the microwave absorption. The change of the microwave absorption at this transition is frequency dependent. The curves taken at a frequency around 25 GHz are the most sensitive to this transition as they demonstrate the largest hysteresis around H_{c3}.

For $H\|C^3$, two branches of the resonance are clearly seen. The frequency of the first branch rises with the field, while the frequency of the second branch decreases (see Figs. 8 and 10). The frequencies of these two branches are

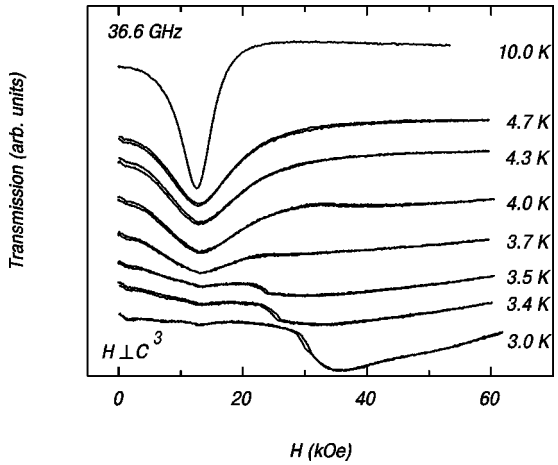

FIG. 7. Temperature evolution of the 36.6 GHz ESR line in $RbFe(MoO_4)_2$ at cooling through the critical region and Néel point.

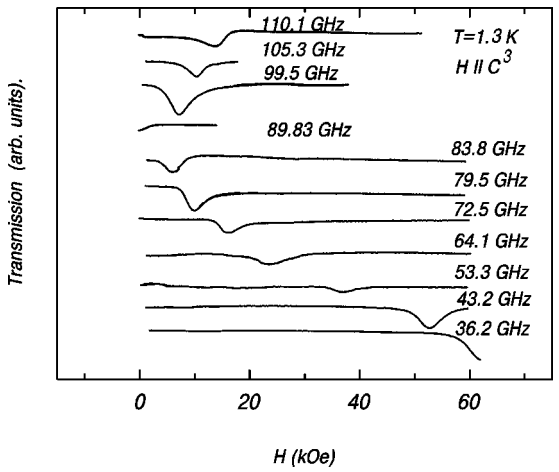

FIG. 8. Magnetic resonance lines in $RbFe(MoO_4)_2$ at different frequencies at $H \| C^3$, $T=1.3$ K.

monotonic functions of the applied magnetic field as expected for the umbrellalike structure.

For $H \perp C^3$, a complicated nonmonotonic dependence of the resonant frequencies ν_i with varying magnetic field was observed (see Fig. 11). The frequency-field curves contain abrupt changes at the fields of the phase transitions in accordance with the data of the magnetization measurements. The values of the phase-transition fields derived from the microwave-absorption curves are marked on the phase diagram in Fig. 6 by filled squares and are in a good agreement with the results of static magnetization measurements. The total number of the observed spin resonance modes is 5.

IV. DISCUSSION

A. Basic principles

The observation of the sequence of the phase transitions for the magnetic field lying in the basal plane implies that there is an easy-plane type of anisotropy (an easy-axis anisotropy would result in the umbrellalike spin structure at $H \perp C^3$ without the cascade of field-induced phase transitions). At the moment there is no explanation for the nature of the incommensurate modulation observed in Ref. 16. Given that there is only a small deviation from an antiparallel alignment of spins in neighboring planes, we propose a model for the field-dependent spin structure in the approximation of a perfect antiferromagnetic orientation of spins in neighboring layers in the zero-field ground state.

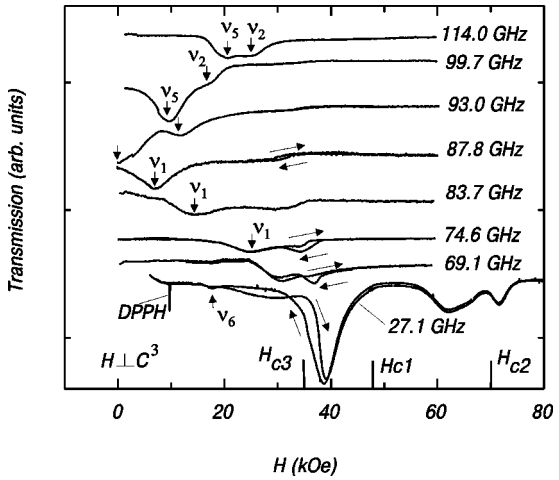

FIG. 9. Magnetic resonance lines in $RbFe(MoO_4)_2$ at different frequencies at $H \perp C^3$, $T=1.3$ K.

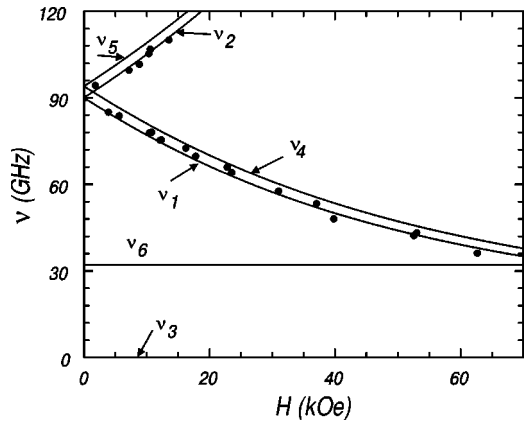

FIG. 10. ESR frequency of $RbFe(MoO_4)_2$ vs magnetic field for $H \| C^3$, $T=1.3$ K. The curves are calculated dependencies after Eqs. (A8),(A9) parameters are described in the text, and filled circles represent the experimental data.

Thus, we consider the following model spin-Hamiltonian, following the notation of Ref. 5:

$$\mathcal{H}=2J\sum_{(ij),n} S_{in}S_{jn}+2J'\sum_{in} S_{in}S_{in+1}+D\sum_{in} (S_{in}^z)^2 - g\mu_B H\sum_{in} S_{in}. \quad (1)$$

Here the sums are taken within the layers (i,j) and along the transverse direction (n), and $D>0$ is the constant of the anisotropy of the easy-plane type.

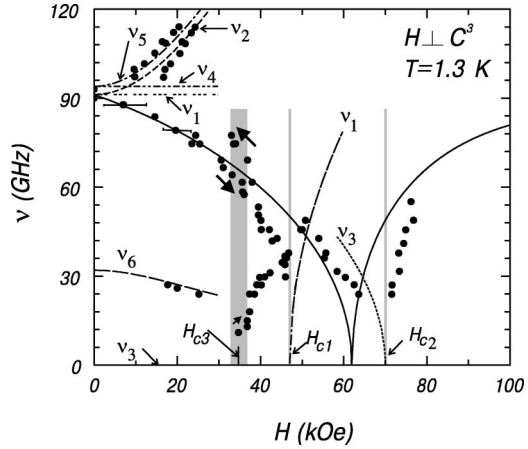

FIG. 11. ESR frequency of $RbFe(MoO_4)_2$ vs magnetic field for $H \perp C^3$, $T=1.3$ K. Dashed curves represent the calculation after Eqs. (A5), (A6), (B7), (B8), solid curves, after Eqs. (B1), (B6). Gray-shadowed bars represent the fields of phase transitions.

B. Field-induced phase transitions and molecular fields

Using the molecular-field calculations[5] of the susceptibilities along and perpendicular to the C^3 axis

$$\chi_{\parallel}=\frac{(g\mu_B)^2}{18J+2D}N,$$

$$\chi_{\perp}=\frac{(g\mu_B)^2}{18J}N$$

(N is the number of magnetic ions), we can estimate the strength of the exchange field H_E and the anisotropy field H_A:

$$H_E=\frac{6JS}{g\mu_B}=67 \text{ kOe},$$

$$H_A=\frac{DS}{g\mu_B}=(5\pm 1.5) \text{ kOe}.$$

The value of H_E is in a good agreement with the saturation field value $H_{\text{sat}}=186$ kOe measured in Ref. 14 (according to the molecular-field calculations $H_{\text{sat}}=3H_E$).

The nearly vanishing slope in the $M(H)$ curve in the field range between H_{c1} and H_{c2} indicates the presence of magnetization plateau and suggests that we should treat this phase as the collinear phase (phase C of Fig. 1), which is stabilized in the range $H_{c1}<H<H_{c2}$ by thermal and quantum fluctuations.[2,5,6] Using the J value derived from the susceptibility measurements and the ratio J'/J derived from the magnetic resonance spectra (see the next section) we can propose a sequence of phase transition on the basis of the model of Ref. 8, where the calculated phase diagram at $T=0$ is plotted on the $H/J, J'S/J$ plane. At the consideration of that phase diagram one should remember that our situation of the easy-plane anisotropy should be considered neglecting the umbrellalike phase derived for the isotropic approximation. For our case of $J'S/J=0.095$ with an easy plane anisotropy this phase diagram predicts a sequence of phase transitions $B1$-$B2$-C-$D1$-$D2$ in the magnetic field. Thus, according to the theoretical analysis of Ref. 8, we can propose that in the field H_{c3} we have transition such as $B1$-$B2$ with change in the mutual orientation of spins in neighboring layers, then transition $B2$-C at $H=H_{c1}$ and C-$D1$ at $H=H_{c2}$. Thus we propose the observed sequence $P1$-$P2$-$P3$-$P4$ may be treated as $B1$-$B2$-C-$D1$.

It should be noticed that the phase boundary observed in the temperature range 3.4–4.2 K and in fields above H_{c2} cannot be smoothly extrapolated to the saturation field 186 kOe at $T=1.3$ K. Therefore, the existence of yet another phase transition at higher magnetic field cannot be ruled out. According to the analysis given in Ref. 8, the phase $D2$ is energetically favorable for certain values of the interplanar exchange in a field just below the saturation field. Thus we suggest the phase $D2$ may, probably, exist below the saturation field.

Using only the results of magnetization and ESR measurements we cannot distinguish between the phases $B1$, $B2$, $B3$ and between the $D1$ and $D2$ phases. Thus, an alternative sequence of phase transitions, such as $B2$-$B3$-C-$D1$ (Ref. 18) should, in principle, also be considered as an explanation of the observed sequence $P1$-$P2$-$P3$-$P4$. A scenario for the field-induced transitions with $B2$ as the starting phase is also suggested on the basis of the molecular field approximation in Ref. 4. The tiny differences between the free energies of the phases $B1$ and $B2$ may be associated with the contribution of thermal and quantum fluctuations which should be taken into account along with the anisotropy. In any case, the exact solution of this problem will only have a limited significance for $RbFe(MoO_4)_2$ because of the incommensurate modulation mentioned, which is still not included in the theoretical models.

Nevertheless, the observation of the H_{c3}-phase transition clearly marks the effect of the interplanar exchange on the field-dependent phases of the AFMT with weakly coupled layers. The observed boundaries in the collinear phase range may be compared to the calculations[5] performed using an isotropic ($D=0$) and XY (infinite D) models at $T=0$ K. The calculated zero-temperature field ranges of the C phase (using $H_E=67$ kOe) are shown in the phase diagram in Fig. 6 by the line segments. There is a qualitative agreement with our observations.

C. Spin-resonance modes

For a triangular system with antiferromagnetic interplane exchange interactions, there should be five resonance modes with nonzero frequencies (the frequency of the sixth mode is zero in small fields in absence of any in-plane anisotropy). We have observed all five resonances for $H\perp C^3$. For weak magnetic fields, where the exchange triangular spin configuration is only slightly distorted, the resonance frequencies may be calculated following the macroscopic theory based on a classical Lagrange formalism.[7] This method of calculation is suitable for complicated and multisublattice systems, however, it is valid only in the field range where the exchange magnetic structure is not strongly distorted by the magnetic field.[19] The basic principles of the calculations and the resulting formulas are given in Appendix A, while the field-dependencies of the resonant frequencies ν_i are presented in Figs. 10 and 11 (the values of the parameters will be described below). For the modes $\nu_{3,6}$ in the low-field range, the oscillating components lie within the plane. The modes with frequencies $\nu_{1,2,3}$ correspond to the in-phase oscillations of spins in the neighboring planes while for the modes with frequencies $\nu_{4,5,6}$, the spins in the neighboring planes oscillate out of phase. Note that for a purely 2D AFMT only the modes $\nu_{1,2,3}$ are present.

The frequencies calculated in this way are only valid for small magnetic fields, when the exchange triangular structure is not strongly distorted. Thus the approximation used is not strictly true in fields of the order of H_{c1}. The distortion of the triangular structure, as shown in the 2D approximation,[5] will result in a field dependence of the resonance frequencies ν_1, ν_3. The approximate correspondence between the parameters of the macroscopic theory described in Appendix A and of the spin-Hamiltonian may be derived using estimates (i.e.,

neglecting zero-point fluctuations) for the susceptibility and resonance frequencies derived for 2D AFMT in the molecular-field approximation

$$a^2 = 18JDS^2 = \gamma^2 3H_A H_E, \tag{2}$$

$$c^2 = \gamma^2 H_E^2 \frac{J'}{J}, \tag{3}$$

where $\gamma = g\mu_B/2\pi\hbar$.

The nonzero frequency of the mode ν_6 confirms the interplanar exchange. Another indication of the interplanar exchange is the splitting of the rising ESR mode (the difference in resonance fields of the modes ν_2 and ν_5 in Fig. 11).

The five spin resonance branches shown in the low-field range in Fig. 11 and the resonance frequencies for $\mathbf{H} \| C^3$ (Fig. 10) may be reasonably described by the Eqs. (A5)–(A9) with only two fitting parameters $a = 90.8$ GHz and $c = 32$ GHz. The dashed curves in Fig. 11 and curves in Fig. 10 are calculated in this way with the anisotropy parameter of the susceptibility, $\eta = 0.05$, derived from the susceptibility measurements.

Using the value of the susceptibility described above and the molecular-field relations (2), (3) we can evaluate the molecular fields and parameters of the Hamiltonian: $H_E = 67$ kOe, $H_A = 5.2$ kOe, $J'/J = 0.039$. These values of H_E and H_A are in reasonable agreement with the values derived from the susceptibility and saturation field.

For $H \perp C^3$, the triangular spin structure of $RbFe(MoO_4)_2$ is already strongly distorted in a field of about 10 kOe. Therefore the macroscopic theory of magnetic dynamics given in Ref. 7 cannot be used. To have at least an approximate description of the resonant frequencies over wider range of applied fields, we used the calculations for the three-sublattice 2D model (i.e., for $J' = 0$) in a classical approximation.[5] The results of these calculations [relations (B1), (B6)] are presented in Fig. 11 by the solid lines. The values of D and J used to calculate these curves are taken from the values of H_E and H_A given above and thus agree with the parameters used for fitting the data in low fields according to relations (A5)–(A9).

For qualitative description of the resonance frequencies within the field range of the collinear phase $H_{c1} < H < H_{c2}$, one should take into account the zero-point fluctuations stabilizing this phase in that field range. The appropriate calculation was made in the $J' = 0$ approximation with the assumptions of the XY model in the same paper of Chubukov and Golosov.[5] Corresponding relations for the lowest resonance frequencies are given in Appendix B [relations (B7), (B8)] and are plotted by dashed lines in the region $H_{c1} < H < H_{c2}$ in Fig. 11. These formulas reveal critical softening of the resonance frequencies near the fields H_{c1} and H_{c2}. We observe a soft mode near H_{c2} which is in qualitative agreement with relation (B8).

V. CONCLUSION

A sequence of field-induced phase transitions, governed by the intraplane exchange interaction and by the weak interplane exchange was found in $RbFe(MoO_4)_2$, a quasi-2D antiferromagnet on a triangular lattice. The magnetic properties may, in part, be explained in terms of a 2D antiferromagnet on a triangular lattice. However, a phase transition governed by weak interplane exchange was found. This phase transition is accompanied by the changes in spin-resonance spectra. A self-consistent description of the magnetization curves, phase transitions and resonance modes in a wide field range is given.

ACKNOWLEDGMENTS

We kindly acknowledge V. I. Marchenko for making calculations of resonance spectra and discussions, S. E. Korshunov, M. E. Zhitomirsky, A. V. Chubukov, and S. S. Sosin for numerous discussions, M. R. Lees for a critical reading of the manuscript and C. Broholm for transmitting to us the results of the unpublished work (Ref. 16). We acknowledge the support of the Russian Foundation for Basic Research (RFBR), Grant No. 01-02-17557, and by Grant No. RP1-2097 of the U.S. Civilian Research and Development Foundation for the Independent States of the former Soviet Union (CRDF).

APPENDIX A: SPIN RESONANCE MODES IN THE MACROSCOPIC APPROACH

We consider 120°-triangular structures in planes 1 and 2, which can be represented by normalized spin densities

$$\mathbf{S}_1(\mathbf{r}) = \mathbf{l}_{11}\cos\mathbf{q}\cdot\mathbf{r} + \mathbf{l}_{12}\sin\mathbf{q}\cdot\mathbf{r},$$

$$\mathbf{S}_2(\mathbf{r}) = \mathbf{l}_{21}\cos\mathbf{q}\cdot\mathbf{r} + \mathbf{l}_{22}\sin\mathbf{q}\cdot\mathbf{r}. \tag{A1}$$

Here $\mathbf{l}_{11}, \mathbf{l}_{12}$ and $\mathbf{l}_{21}, \mathbf{l}_{22}$ are two pairs of orthogonal unit vectors of antiferromagnetism $q_x = 4\pi/3a$, $q_y = 0$, where a is the crystal period within the plane and vector $\mathbf{r}$ takes discrete values within the basal plane pointing at the magnetic sites on a triangular lattice. This structure is due to the in-plane exchange. The mutual orientation of spin triangles in neighboring planes for weak interplane exchange corresponds to the minimum of the Heisenberg exchange energy of nearest neighbors from different planes

$$\alpha(\mathbf{l}_{11}\mathbf{l}_{21} + \mathbf{l}_{12}\mathbf{l}_{22}). \tag{A2}$$

For $\alpha > 0$: $\mathbf{l}_{11} = -\mathbf{l}_{21}$, $\mathbf{l}_{12} = -\mathbf{l}_{22}$. For $\alpha < 0$: $\mathbf{l}_{11} = \mathbf{l}_{21}$, $\mathbf{l}_{12} = \mathbf{l}_{22}$.

Note, that the low-frequency spectrum, which depends on the quadratic expansion on the angles of the mutual rotation of the spin triangles, is the same for the antiferromagnetic ($\alpha > 0$) and ferromagnetic ($\alpha < 0$) exchange.

The Lagrange function of the spin dynamics has three contributions: two ''ordinary'' terms of the triangular structures of the two systems of spin planes ($\mathbf{l}_{11}, \mathbf{l}_{12}$)

$$\frac{1}{4}\left\{\frac{\chi_\perp}{\gamma^2}(\mathbf{\Omega}_1 + \gamma\mathbf{H})^2 + \frac{\chi_\| - \chi_\perp}{\gamma^2}(\mathbf{\Omega}_1 + \gamma\mathbf{H}, \mathbf{n}_1)^2 + \beta n_{1z}^2\right\} \tag{A3}$$

and ($\mathbf{l}_{21}, \mathbf{l}_{22}$)

$$\frac{1}{4}\left\{\frac{\chi_\perp}{\gamma^2}(\mathbf{\Omega}_2+\gamma\mathbf{H})^2+\frac{\chi_\parallel-\chi_\perp}{\gamma^2}(\mathbf{\Omega}_2+\gamma\mathbf{H},\mathbf{n}_2)^2+\beta n_{2z}^2\right\} \quad \text{(A4)}$$

while the third term, the energy of the interplane exchange, is given above [Eq. (A2)]. Here $\mathbf{n}_1=[\mathbf{l}_{11}\mathbf{l}_{12}]$, $\mathbf{n}_2=[\mathbf{l}_{21}\mathbf{l}_{22}]$ are unit vectors in the spin space, which are normal to the spin planes, β is the constant of uniaxial anisotropy, and $\mathbf{\Omega}_1$ and $\mathbf{\Omega}_2$ are angular velocities of rotation of the spin triangles. The values $\chi_\parallel$ and $\chi_\perp$ determine the components of the tensor of the magnetic susceptibility in the ground state, along and perpendicular to the vector $\mathbf{n}_1$, respectively.

For the in-plane field, the frequencies of the in-phase oscillations of spins in neighboring planes are given by

$$\nu_1=a,$$
$$\nu_2=\sqrt{a^2+H^2}, \quad \text{(A5)}$$
$$\nu_3=0.$$

The additional frequencies due to the interplane exchange (spins of different planes oscillate ''out of phase'') are

$$\nu_4=b=\sqrt{a^2+A^2},$$
$$2\nu_{5,6}^2=b^2+c^2+H^2\pm\sqrt{(b^2+c^2+H^2)^2-4c^2(b^2-\eta H^2)}. \quad \text{(A6)}$$

Here $A^2=\gamma^2\alpha/\chi_\perp$, $a^2=\gamma^2\beta/\chi_\perp$, $\eta=(\chi_\parallel-\chi_\perp)/\chi_\perp$, $c^2=2A^2/(1+\eta)$. Parameters a, b, and c are coupled by the relation

$$2(b^2-a^2)=(1+\eta)c^2. \quad \text{(A7)}$$

For the magnetic field oriented parallel to the C^3 axis, ordinary resonances (in-phase motion of triangles) are

$$\nu_{1,2}=\sqrt{a^2+\left(\frac{1+\eta}{2}\gamma H\right)^2}\pm\frac{1-\eta}{2}\gamma H, \quad \text{(A8)}$$
$$\nu_3=0,$$

while the additional frequencies (the triangles rotate in opposite directions) are

$$\nu_{4,5}=\sqrt{b^2+\left(\frac{1+\eta}{2}\gamma H\right)^2}\pm\frac{1-\eta}{2}\gamma H, \quad \text{(A9)}$$
$$\nu_6=c.$$

APPENDIX B: SPIN-RESONANCE MODES IN THE 2D MODEL (REF. 5)

1. Molecular field approximation

Introducing the normalized field

$$h=\frac{2\mu_B H}{6JS}=3H/H_{\text{sat}}$$

we have the following resonance frequencies, for the magnetic field lying in the easy plane of 2D-AFMT.

(1) Below the transition to the collinear phase ($0<h<1$)

$$\nu_1=\frac{6JS}{2\pi\hbar}\left[\frac{D}{6J}(3-2h-h^2)\right]^{1/2}, \quad \text{(B1)}$$

$$\nu_2=\frac{6JS}{2\pi\hbar}\left[\frac{D}{6J}(3+2h+h^2)\right]^{1/2}, \quad \text{(B2)}$$

$$\nu_3=0. \quad \text{(B3)}$$

(2) Above the transition to the canted phase ($1<h<3$)

$$\nu_1=0, \quad \text{(B4)}$$

$$\nu_2=\frac{6JS}{2\pi\hbar}\left[\frac{D}{6J}\frac{(h^6-3h^4+35h^2+63)}{16h^2}\right)^{1/2}, \quad \text{(B5)}$$

$$\nu_3=\frac{6JS}{2\pi\hbar}\left[\frac{D}{6J}\frac{(9-h^2)(h^2-1)(h^2+7)}{16h^2}\right)^{1/2}. \quad \text{(B6)}$$

2. XY-model including fluctuations

The two lowest resonant frequencies in the collinear phase are

$$\nu_1=\frac{6JS}{2\pi\hbar}(h-h_{c1})^{1/2}, \quad \text{(B7)}$$

$$\nu_3=\frac{6JS}{2\pi\hbar}\left(\frac{h_{c2}-h}{3}\right)^{1/2}. \quad \text{(B8)}$$

Here h_{c1} and h_{c2} are the normalized values of the critical fields H_{c1} and H_{c2}.

[1] H. Kawamura and S. Miyashita, J. Phys. Soc. Jpn. **54**, 4530 (1985).
[2] S. E. Korshunov, J. Phys. C **19**, 5927 (1986).
[3] P. W. Anderson, Science **235**, 1196 (1987).
[4] M. L. Plumer and A. Caille, Phys. Rev. B **42**, 10 388 (1990).
[5] A. V. Chubukov and D. I. Golosov, J. Phys.: Condens. Matter **3**, 69 (1991).
[6] E. Rastelli and A. Tassi, J. Phys.: Condens. Matter **8**, 1811 (1996).
[7] A. F. Andreev and V. I. Marchenko, Usp. Fiz. Nauk **130**, 39 (1980) [Sov. Phys. Usp. **23**, 21 (1980)].
[8] R. S. Gekht and I. N. Bondarenko, Zh. Éksp. Teor. Fiz. **111**, 627 (1997) [JETP **84**, 345 (1997)].
[9] M. E. Zhitomirsky, O. A. Petrenko, and L. A. Prozorova, Phys. Rev. B **52**, 3511 (1995).
[10] S. Schmidt, B. Wolf, M. Sieling, S. Zvyagin, I. Kouroudis, and B. Lüthi, Solid State Commun. **108**, 509 (1998).

[11] H. Kadovaki, H. Ieda, H. Kadovaki, and K. Ubikoshi, J. Phys. Soc. Jpn. **52**, 2882 (1983).
[12] S. Angelov and J. P. Doumerc, Solid State Commun. **77**, 213 (1991).
[13] M. F. Collins and O. A. Petrenko, Can. J. Phys. **75**, 605 (1997).
[14] T. Inami, Y. Ajito, and T. Goto, J. Phys. Soc. Jpn. **65**, 2374 (1996).
[15] M. N. Popova, S. A. Klimin, P. H. M. van Loosdrecht, B. N. Mavrin, L. A. Prozorova, A. I. Smirnov, L. E. Svistov, A. Ya. Shapiro, and L. N. Demianets (unpublished).
[16] G. Gasparovich, M. Kenzelmann, C. Broholm, L. N. Demianets, and A. Ya. Shapiro (unpublished).
[17] H. Serrano-Gonzalez, S. T. Bramwell, K. D. M. Harris, B. M. Kariuki, L. Nixon, I. P. Parkin, and C. Ritter, Phys. Rev. B **59**, 14 451 (1999).
[18] S. E. Korshunov (private communication).
[19] The authors acknowledge V. I. Marchenko for making these calculations.